Influence of Inertia and Viscoelasticity in Entry Flows Through an Abrupt Annular Contraction

E. MITSOULIS, *Department of Chemical Engineering, University of Ottawa, Ottawa, Ontario K1N 9B4, Canada*

Synopsis

A numerical simulation of entry flows in an annular die has been undertaken for Newtonian and power-law fluids as well as viscoelastic fluids that exhibit normal stresses in shear flow. Experimentally measured normal stress and viscosity data are included in a simple rheological model. The influence of inertia and viscoelasticity are examined separately as functions of the Reynolds (Re) and Weissenberg (Ws) numbers. It is found that inertia decreases the size of the corner vortices in the reservoir corners which tend to increase rapidly with elasticity level in the absence of inertia. The combined effect of inertia and elastic forces is to first increase the vortex size followed by a decrease at higher Re numbers. The numerical simulations are in qualitative agreement with experimental studies available in the literature.

INTRODUCTION

The flow of polymer solutions and melts through processing equipment is of considerable interest in the polymer processing industry. These fluids exhibit unusual behavior when flowing in nontrivial geometries, such as abrupt contractions. Experimental investigations abound in the literature for a variety of polymer solutions and melts and have been reviewed quite recently.[1] On the other hand, the corresponding numerical simulations have had an equal growth and there exist numerous reports that deal with the prediction of flow patterns in contractions. Again, a thorough and systematic literature survey can be found in the review by White et al.[1]

The major difficulty for the theoretical, and hence, numerical analysis is the lack of well-accepted constitutive equations that can adequately describe the flow of viscoelastic materials. While the case for purely viscous (inelastic) materials has been quite adequately handled by the generalized Newtonian fluid, the case of viscoelasticity still remains an open subject. To date, it seems that the only successful simulations for flow through abrupt contractions and prediction of extrudate swell for polymer solutions and melts have been based on a rather heuristic approach that assumes the flow to be locally steady-shear (viscometric approximation approach).[2,3] This method uses the minimum amount of rheological information (i.e., shear viscosity and normal stress data which can be obtained experimentally) to at least qualitatively simulate strong viscoelastic behavior exhibited by several test fluids.

Almost all works, both experimental and theoretical, that have been performed on contractions deal with the entry flow from a reservoir into a planar

Journal of Applied Polymer Science, Vol. 37, 627–643 (1989)
 CCC 0021-8995/89/030627-17$04.00

(slit) or tubular (capillary) die.[4] In many cases, the nonlinearities caused either by inertia terms (non-zero Reynolds number flows) or by viscoelastic terms (non-zero Weissenberg number flows) have been separated for a better understanding of the effects. Therefore, a variety of simulations exists that deal with:

1. Creeping flow of Newtonian and generalized Newtonian (shear-thinning) fluids (Re = 0, Ws = 0)[5-7]
2. Noncreeping flow of Newtonian and generalized Newtonian (shear-thinning) fluids (Re $\neq$ 0, Ws = 0)[8,9]
3. Creeping flow of viscoelastic fluids (Re = 0, Ws $\neq$ 0)[2,3,10]
4. Noncreeping flow of viscoelastic fluids (Re $\neq$ 0, Ws $\neq$ 0)[11,12]

The planar and tubular entry flows are of importance in various industrial applications, such as synthetic fiber spinning and sheet and rod extrusion of plastic products. However, the processing of viscoelastic fluids in geometries other than circular ducts has taken on added significance. One such geometry is the annulus. Annular entry flows are encountered in the extrusion of plastic tubes, in wire coating, in film blowing, and in annular rheometers.

Two experimental investigations have been performed on the entry flow of fully characterized polymer solutions in annular dies. One deals with entry flow in a straight annulus,[13] while the other is concerned with the flow patterns in an abrupt 2:1 concentric annular contraction.[14] Since no numerical attempt has been made to date to analyze such a flow field, it is the purpose of this article to perform the corresponding simulations and investigate the roles that inertia and viscoelasticity play in the flow of certain polymer solutions in such geometries. The results are compared with experimental findings for two test fluids for which steady-shear data are available for the viscosity and the normal stresses.

MATHEMATICAL MODELING

The isothermal, incompressible, laminar flow of polymer solutions and melts can be fully described by the equations of conservation of mass and momentum (including the inertia terms):

$$\nabla \cdot \mathbf{v} = 0 \tag{1}$$

$$\rho \mathbf{v} \cdot \nabla \mathbf{v} = -\nabla p + \nabla \cdot \tau \tag{2}$$

where $\mathbf{v}$ is the velocity vector, ρ is the density, p is the pressure, and τ is the extra stress tensor.

For axisymmetric flows, such as these encountered in tubular and annular geometries, a cylindrical coordinate system (r-z-θ) may be used and the three-dimensional problem is reduced to two dimensions, namely r and z (assuming no variations in the θ-direction). The conservation equations are

then written as[15]:

$$\frac{\partial v_r}{\partial r} + \frac{v_r}{r} + \frac{\partial v_z}{\partial z} = 0 \tag{3}$$

$$\rho\left(v_r\frac{\partial v_r}{\partial r} + v_z\frac{\partial v_r}{\partial z}\right) = -\frac{\partial p}{\partial r} + \frac{\partial \tau_{rr}}{\partial r} + \frac{\tau_{rr}}{r} + \frac{\partial \tau_{zr}}{\partial z} - \frac{\tau_{\theta\theta}}{r} \tag{4}$$

$$\rho\left(v_r\frac{\partial v_z}{\partial r} + v_z\frac{\partial v_z}{\partial z}\right) = -\frac{\partial p}{\partial z} + \frac{\partial \tau_{rz}}{\partial r} + \frac{\tau_{rz}}{r} + \frac{\partial \tau_{zz}}{\partial z} \tag{5}$$

The extra stress tensor τ is, in general, given by some constitutive equation, which complies with the rules of tensorial invariance and objectivity of the stresses to the frame of reference.[16] However, due to the lack of such a widely accepted constitutive equation that can adequately describe the flow of polymer solutions and melts, we will use instead the viscometric approximation theory (VAT),[3] that basically corrects the stresses of a generalized Newtonian fluid to account for normal stress measurements in shear flows. For axisymmetric geometries, the components of τ are then given by:[3]

$$\tau_{rr} = \eta\dot{\gamma}_{rr} + \Psi_2\dot{\gamma}_{rz}^2 \tag{6a}$$

$$\tau_{\theta\theta} = \eta\dot{\gamma}_{\theta\theta} \tag{6b}$$

$$\tau_{zz} = \eta\dot{\gamma}_{zz} + (\Psi_1 + \Psi_2)\dot{\gamma}_{rz}^2 \tag{6c}$$

$$\tau_{rz} = \tau_{zr} = \eta\dot{\gamma}_{rz} \tag{6d}$$

where η is the apparent viscosity and Ψ_1 and Ψ_2 the first and second normal stress coefficients, respectively. These are, in general, functions of the magnitude $|\dot{\gamma}|$ of the rate-of-strain tensor $\dot{\gamma} = \nabla\mathbf{v} + \nabla\mathbf{v}^T$, given by:

$$|\dot{\gamma}| = \left[\tfrac{1}{2}\left(\dot{\gamma}_{rr}^2 + \dot{\gamma}_{\theta\theta}^2 + \dot{\gamma}_{zz}^2 + 2\dot{\gamma}_{rz}^2\right)\right]^{1/2} \tag{7}$$

where

$$\dot{\gamma}_{rr} = 2\frac{\partial v_r}{\partial r}, \quad \dot{\gamma}_{\theta\theta} = 2\frac{v_r}{r}, \quad \dot{\gamma}_{zz} = 2\frac{\partial v_z}{\partial z}, \quad \dot{\gamma}_{rz} = \dot{\gamma}_{zr} = \frac{\partial v_r}{\partial z} + \frac{\partial v_z}{\partial r} \tag{8}$$

Equations (6a–d) give rise to the following viscometric functions:

$$\tau_{rz} = \eta\dot{\gamma}_{rz} \tag{9a}$$

$$N_1 = \tau_{zz} - \tau_{rr} = \Psi_1\dot{\gamma}_{rz}^2 \tag{9b}$$

$$N_2 = \tau_{rr} - \tau_{\theta\theta} = \Psi_2\dot{\gamma}_{rz}^2 \tag{9c}$$

where τ_{rz} is the shear stress and N_1, N_2 the first and second normal stress

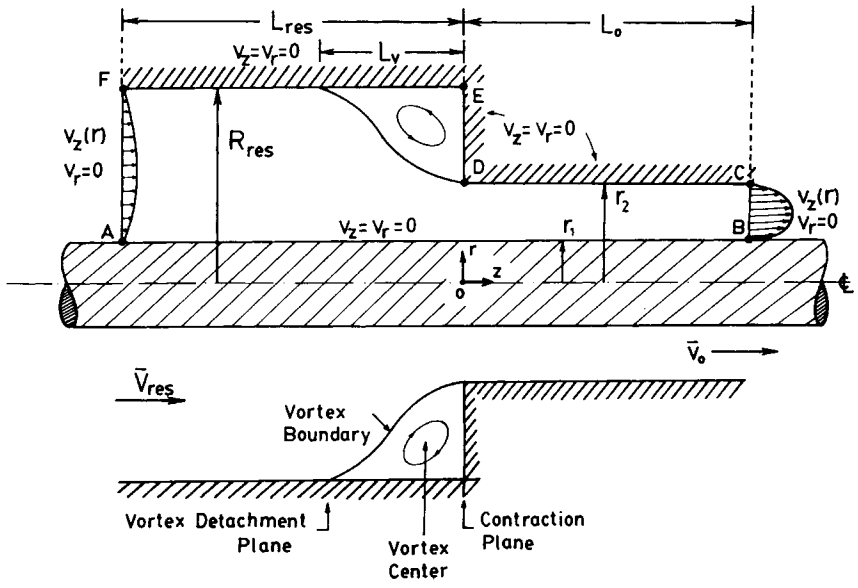

Fig. 1. Schematic diagram and notation for a 2 : 1 annular entry flow geometry.

differences, respectively. Note that for a purely viscous (inelastic) fluid, $\Psi_1 = \Psi_2 = 0$ (or $N_1 = N_2 = 0$), and Eqs. (6a–d) reduce to these for the generalized Newtonian fluid. Furthermore, if η = constant, we obtain the equations for a Newtonian fluid.

The viscometric functions obtained from steady-shear experiments for polymer solutions or melts are usually related to the shear rate $\dot{\gamma}$ by the power-law model:[14]

$$\tau = m\dot{\gamma}^n \tag{10}$$

$$N_1 = A\dot{\gamma}^b \tag{11}$$

Since it is well known that the second normal stress difference N_2 is much smaller than N_1,[17,18] we have used in what follows $N_2 = 0$ ($\Psi_2 = 0$).

In an annular geometry and referring to Figure 1, it is appropriate to define a hydraulic radius r_H:

$$r_H = \frac{r_2 - r_1}{2} \tag{12}$$

where r_1 and r_2 are the inner and outer radii of the downstream annulus, respectively. Then, for a fully developed flow in the downstream annulus, one obtains an equivalent hydraulic shear stress τ_H:

$$\tau_H = \left(\frac{dp}{dz}\right)_o r_H \tag{13}$$

where $(dp/dz)_o$ is the pressure gradient in the annulus; the equivalent hydraulic shear rate $\dot{\gamma}_H$ for power-law fluids is given by:

$$\dot{\gamma}_H = \left[\frac{1}{m}\left(\frac{dp}{dz}\right)_o r_H\right]^{1/n} \tag{14}$$

The relevant dimensionless groups for power-law fluids obeying eqs. (10) and (11) are then defined as follows:[14]
Reynolds number,

$$\mathrm{Re} = \frac{2^{3-n} r_H^n \mathbf{v}_o^{2-n} \rho}{m\left[(\epsilon_0 n + \epsilon_1)/n\right]^n} = \frac{\text{inertia forces}}{\text{viscous forces}} \tag{15}$$

Weissenberg number,

$$\mathrm{Ws} = \frac{A}{m}\left(\frac{\mathbf{v}_o}{r_H}\right)^{b-n} = \frac{\text{elastic forces}}{\text{viscous forces}} \tag{16}$$

Elasticity number,

$$\xi = \frac{\mathrm{Ws}}{\mathrm{Re}} = \frac{\text{elastic forces}}{\text{inertia forces}} \tag{17}$$

In the above, $\mathbf{v}_o$ is the average velocity in the downstream annulus, readily obtained from the flow rate Q according to:

$$Q = \pi \mathbf{v}_o\left(r_2^2 - r_1^2\right) \tag{18}$$

The values of the geometric parameters ϵ_0 and ϵ_1 depend on the ratio $\kappa = r_1/r_2$ and are given by Kozicki and Tiu.[19]

The vortex detachment length L_v, is represented in dimensionless form by:

$$X_v = -\frac{L_v}{4R_H} \tag{19}$$

where R_H is the hydraulic radius of the upstream annulus ($R_H = (R_{\mathrm{res}} - r_1)/2$).

The overall pressure drop ΔP in the system can be used to evaluate the entrance correction n_{en} defined by:

$$n_{en} = \frac{\Delta P - (\Delta P_{\mathrm{res}} + \Delta P_o)}{2\tau_H} \tag{20}$$

where ΔP_{res} is the pressure drop obtained for fully developed annular flow in the reservoir, ΔP_o the corresponding value obtained for the die and τ_H the hydraulic shear stress at the die given by Eq. (13).

For the mathematical analysis, a set of boundary conditions has to be employed. Referring to Figure 1, we have:

along AB, CD, DE, EF, no-slip conditions: $v_z = v_r = 0$
along FA and CB: $v_z = v_z(r), v_r = 0$

Therefore, along the entry and the exit planes, we prescribe the corresponding fully developed velocity profiles, that have to be obtained numerically for the case of a generalized Newtonian fluid (e.g., power-law fluid).[20] Note that only for Newtonian fluids can the profiles be obtained analytically.[15] A standard Newton-Raphson method has been used for the integration of the ordinary differential equation for a fully developed flow in an annulus to provide the corresponding entry and exit velocity profiles for a given flow rate.

Method of Solution

The above conservation and constitutive Eqs. (3)–(6) along with the appropriate boundary conditions (see Fig. 1) are solved by a standard Galerkin/finite-element method (G/FEM). The primary variables are the velocities and pressure (u-w-p formulation). Streamlines are obtained a posteriori by solving the Poisson equation for the stream function. The nonlinear system of equations is solved using the MACVIP finite-element program[21] that employs a frontal solver and uses a direct substitution iterative scheme (Picard method). The solution process starts from the Newtonian field (Stokes problem, Re = 0, Ws = 0), which is used to obtain a first approximation for the velocities, velocity gradients, and stresses. The inertia terms and updated viscosity enter in the element (stiffness) matrix which is now nonsymmetric (Re $\neq$ 0), while the elastic terms involving Ψ_1 and Ψ_2 are treated as effective body forces and enter in the load vector (Ws $\neq$ 0). A continuation scheme is used for increasing values of Re and Ws, in which the initial estimate is the solution for the previous set of Re and Ws numbers (zero-order continuation). More details about the method have been given elsewhere.[9,22]

TEST FLUID PROPERTIES

In this study, two test fluids are considered, for which experimental data are available for shear and normal stresses over a wide range of shear rates.[14,23]

The first test fluid FM1 consists of 0.60% Methocel 90-HG (hydroxypropyl methyl cellulose) in water (ρ = 1 g/cm^3) and exhibited no measurable elastic properties in steady-shear experiments. The shear stress data give rise to the following power-law relationship:

$$\tau = 0.196\dot{\gamma}^{0.862} \quad \text{(Pa)} \tag{21a}$$

$$N_1 = 0 \quad \text{(Pa)} \tag{21b}$$

The second test fluid, FS8, consists of 1.25% Separan MG500 (partially hydrolyzed polyacrylamide) in water (ρ = 1 g/cm^3). The shear stress is given

by:[23]

$$\tau = 4.46\dot{\gamma}^{0.367} \quad \text{(Pa)} \quad \text{for } 4.4 < \dot{\gamma} \leq 222\ \text{s}^{-1} \tag{22a}$$

$$\tau = 3.914\dot{\gamma}^{0.397} \quad \text{(Pa)} \quad \text{for } 222 < \dot{\gamma} < 1112\ \text{s}^{-1} \tag{22b}$$

while the first normal stress difference N_1 is given by:[23]

$$N_1 = 9.269\dot{\gamma}^{0.633} \quad \text{(Pa)} \quad \text{for } 17.6 < \dot{\gamma} \leq 222\ \text{s}^{-1} \tag{22c}$$

$$N_1 = 4.667\dot{\gamma}^{0.758} \quad \text{(Pa)} \quad \text{for } 222 < \dot{\gamma} < 1112\ \text{s}^{-1} \tag{22d}$$

In the above, $\dot{\gamma} = \dot{\gamma}_H$, the hydraulic shear rate given by Eq. (14).

RESULTS AND DISCUSSION

Viscous Inelastic Fluids

The numerical simulations were performed first in the absence of viscoelasticity (Ws = 0) for a Newtonian fluid and the two test fluids FM1 and FS8 in an abrupt 2:1 concentric annular contraction shown in Figure 1. Tan and Tiu[14] present flow pattern photographs for these two fluids, so a direct comparison can be made with the present results.

All calculations were performed with the finite-element grid shown in Figure 2. It consists of 448 triangular elements, 969 nodes (17 nodes across and 57 nodes along the domain), and 1941 unknown degrees of freedom. The

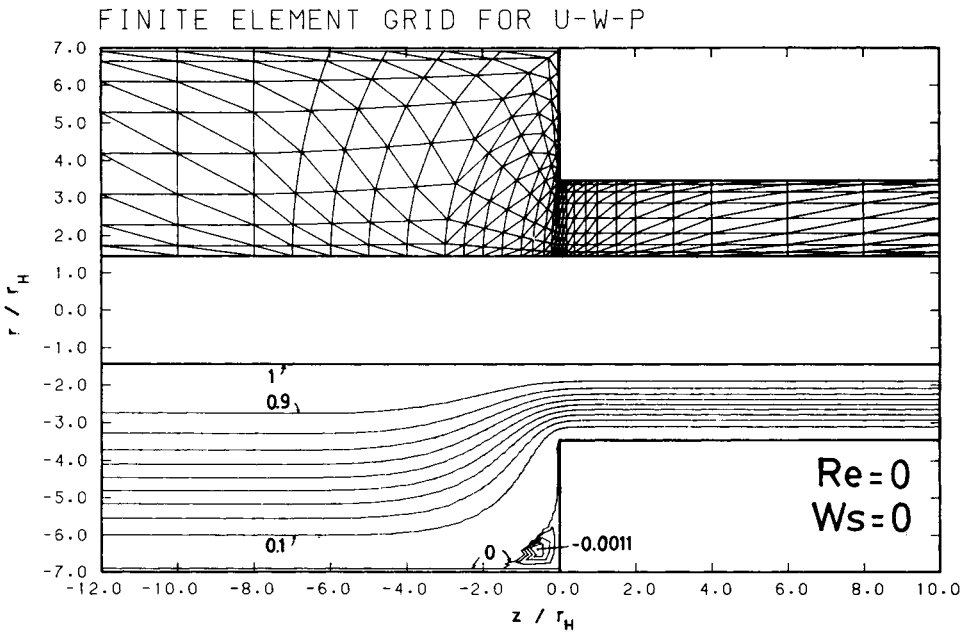

Fig. 2. Finite-element grid for u-w-p formulation (upper half) and streamline pattern for a Newtonian fluid with Re = 0, Ws = 0 (lower half).

present grid resembles the one used earlier,[3] and has a high density of smaller elements near the re-entrant corner to better capture the dramatic changes that occur in the neighborhood of the stress singularity (corner point). The entry and exit lengths have been chosen in such a way, so that the imposition of fully developed velocity profiles is justified far from the contraction.

The Newtonian creeping flow field (Re = 0, Ws = 0) is shown in Figure 2 (lower half). The streamlines have been obtained by normalizing the stream function to take values between 0 (outer wall) and 1 (inner wall) with increments of 0.1 in between. A small vortex appears in the reservoir corner with an intensity of -0.0011 (or 0.11% of the flow rate) and a dimensionless length X_v of 0.135. The entrance correction n_{en} was found to be 0.513 (cf., the values of 0.45 for capillaries and 0.255 for slits in a 2:1 abrupt contraction[7]). The small Newtonian vortex has also been found experimentally in contraction flows.[24]

The influence of inertia on the flow of Newtonian fluids in this particular geometry is illustrated in the sequence of flow patterns of Figure 3. Successive solutions are obtained by incrementing ρ (and therefore Re). Identical results were obtained by incrementing the flow rate through $\mathbf{v}_o$, the average downstream velocity, and keeping ρ constant (thus incrementing Re). Satisfactory convergence was obtained without difficulty up to Re = 1200, provided that adequate step sizes in Re were followed (in this case the runs were performed at Re = 0, 10, 20, 30, 50, 100, 200, 300, 500, 800, 1000, 1200, 1300 with each solution having as an initial guess the solution of the previous Re run). A limit point was reached at 1300, at which no convergence could be obtained with increasing number of iterations. Note that Tan and Tiu[14] also report a highest experimental value of Re = 1308. The adequacy of the solution was judged by the norm of the error which was always less than 0.01 for the converged cases. The radial pressure distribution in fully developed flow at entry was also negligible (the error reached 0.25% for Re = 1200), thus indicating the adequacy of the entry and exit lengths of the domain.

The results of Figure 3 show some interesting phenomena caused solely by inertia. As Re increases, the vortex decreases in size and intensity, in agreement with other findings.[8,9,11] Around Re = 200, a stationary vortex just inside the downstream channel was computed to exist, which increased with Re. This vena contracta has also been found computationally[25] at Re ~ 150–200 in flow through tubular contractions, and experimental evidence also exists (see, e.g., Christiansen et al.[25]). For Re $\geq$ 200, the reservoir corner vortex was also found to increase in size taking an elongated shape. At Re = 1200, the dimensionless vortex length X_v was computed to be 0.21 with an intensity of -0.0015 (or 0.15% of the flow rate) while the vena contracta accounted for 1.1% of the flow rate. This behavior of the reservoir vortex has also been observed by Crochet and Pilate[11] in flow through a 2:1 planar abrupt contraction. However, their work does not corroborate the presence of a vena contracta, which may be a feature found solely in axisymmetric geometries.

The influence of shear thinning for power-law fluids has been examined in the absence of viscoelasticity for fluids FM1 (n = 0.862) and FS8 (n = 0.367, only). The convergence limit was found to be reduced with increasing shear thinning. The highest Re_c values for convergence were Re_c = 1100 for n = 0.862, and Re_c = 600 for n = 0.367.

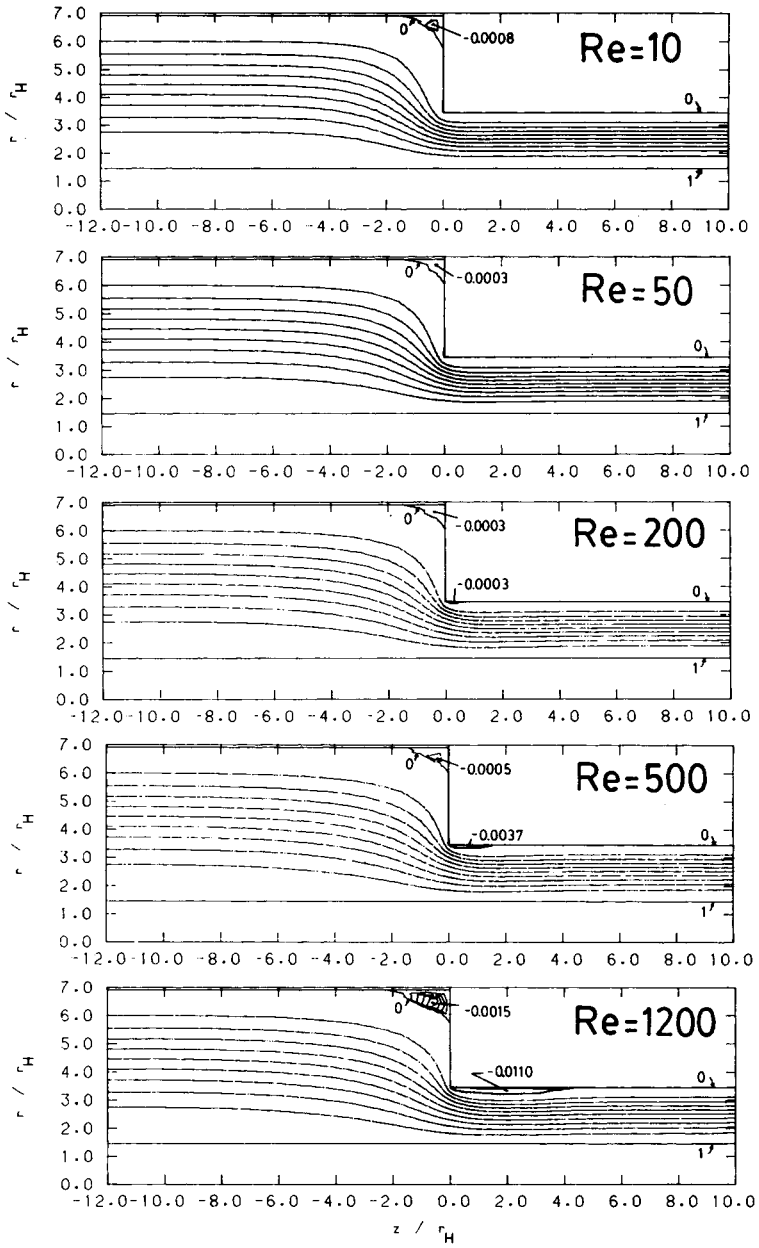

Fig. 3. Flow patterns of a Newtonian fluid for different Re number (2:1 annular abrupt contraction).

Figure 4 shows the corresponding flow patterns for fluid FM1 (power-law fluid with n = 0.862). The results closely resemble those for Newtonian fluids as expected, since the value of n is close to 1 (little shear thinning). The flow pattern for Re = 6 can be directly compared to the experimentally obtained photograph given by Tan and Tiu[14] (cf., their Figure 5). The virtual identity of the experimental and computational flow patterns clearly demonstrates that the entry flow problem for inelastic fluids is solved.[24]

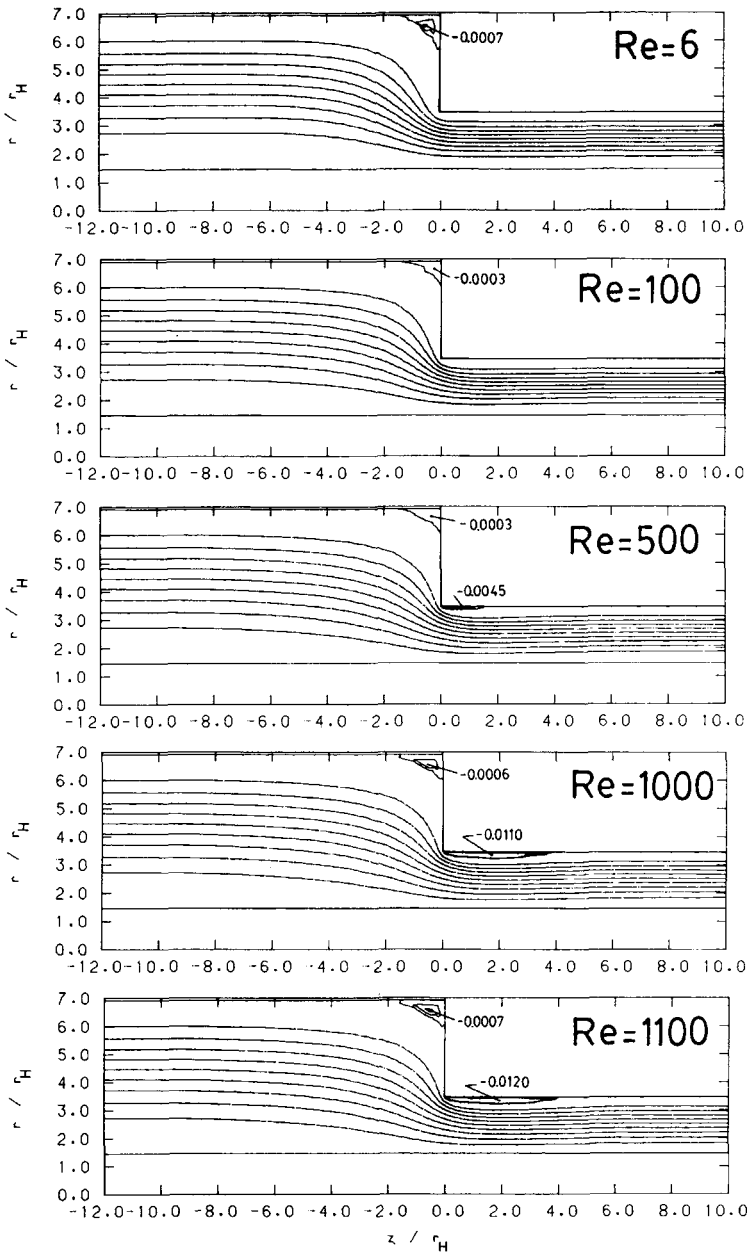

Fig. 4. Flow patterns of a power-law fluid (n = 0.862) for different Re numbers (fluid FM1 in a 2 : 1 annular abrupt contraction).

Figure 5 shows the flow patterns for fluid FS8 (power-law fluid with n = 0.367) in the absence of viscoelasticity (Ws = 0). The results for Re = 1.33, 17.4, 53.5, and 159 correspond to the photographs given by Tan and Tiu[14] (cf., their Figure 4). Clearly, the presence of viscoelasticity in the experiments accounts for the difference in the flow behavior. The same features are found as before, specifically, a reduction in the size of the reservoir corner vortex and

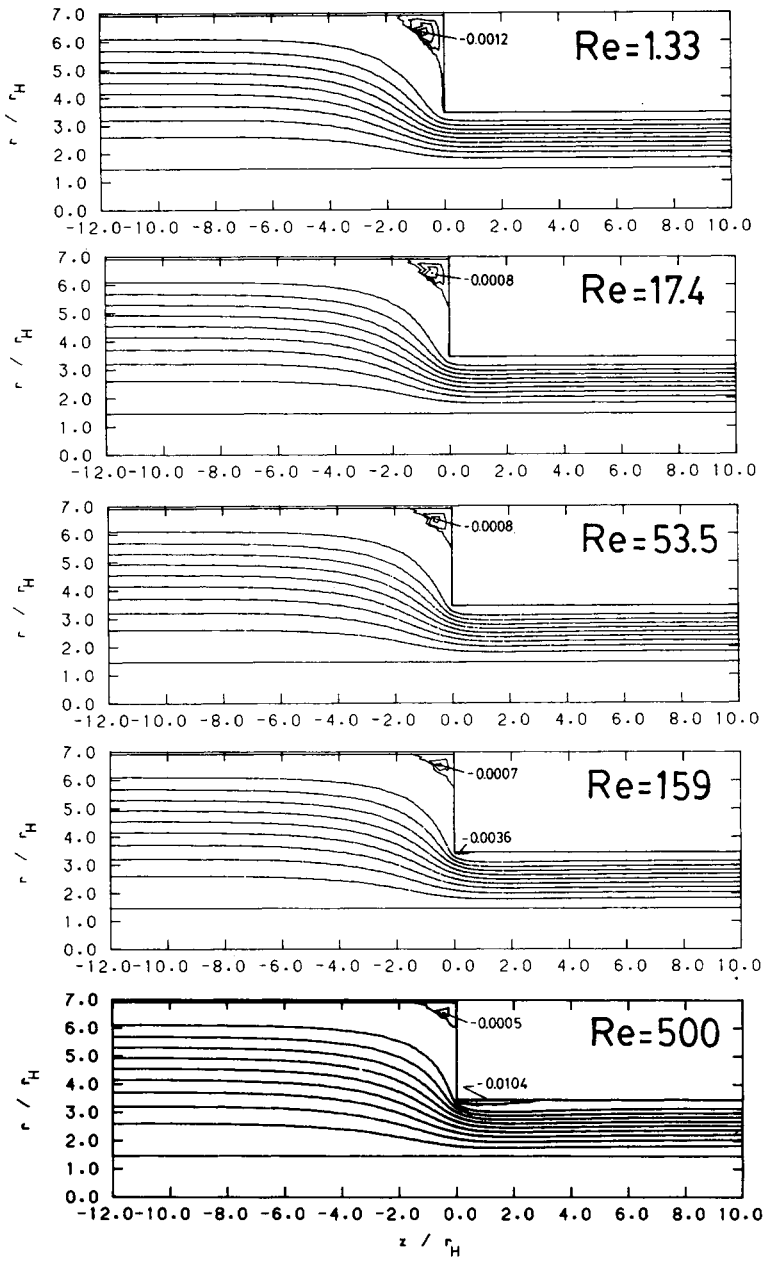

Fig. 5. Flow patterns of a power-law fluid (n = 0.367) for different Re numbers (fluid FS8 with Ws = 0 in a 2 : 1 annular abrupt contraction).

the appearance of a vena contracta at about Re ≈ 150, that grows with increasing Re.

The pressures from the present runs can be used to find the entrance correction n_{en} as given by Eq. (20). The results for Newtonian fluids are shown in Figure 6, along with the asymptotic lines for entry flows from an infinite reservoir into a capillary and a slit. These lines are obtained for low

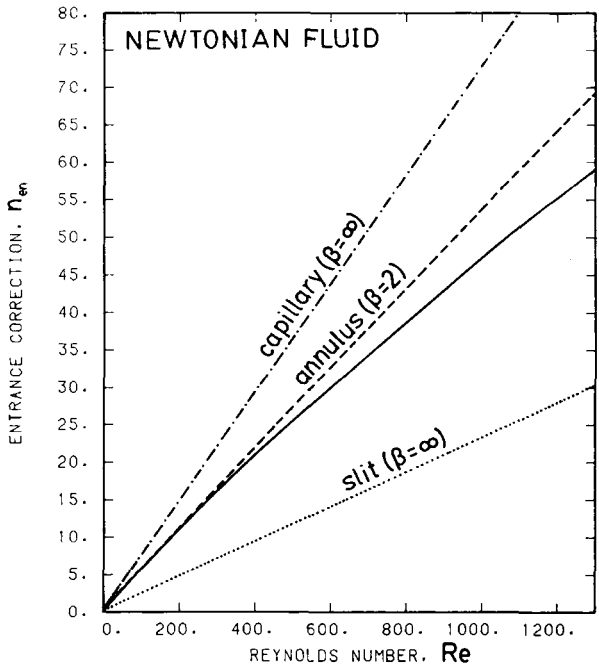

Fig. 6. Entrance correction vs. Re number (Newtonian fluids) (- - -) capillary ($\beta = \infty$); (- - -) annulus ($\beta = 2$); (. . .) slit ($\beta = \infty$). The broken lines correspond to the asymptotes obtained for low Re numbers (Re $\leq$ 100).[9]

Re numbers (Re $\leq$ 100) and follow the equations:[9]

$$(\text{slit}, \beta = \infty) \qquad n_{en} = 0.0225\ \text{Re} + 0.407 \tag{23}$$

$$(\text{capillary}, \beta = \infty) \qquad n_{en} = 0.0709\ \text{Re} + 0.589 \tag{24}$$

where β is the contraction ratio, and $\text{Re} = \rho v_0 D/\mu$ for capillaries and $\text{Re} = \rho v_0 2H/\mu$ for slits. The present results for a 2:1 annular abrupt contraction also exhibit an asymptotic linear dependence with Re at Re $\leq$ 200, according to the equation:

$$(\text{annulus}, \beta = 2) \qquad n_{en} = 0.0526\ \text{Re} + 0.513 \tag{25}$$

The Reynolds number Re for concentric annuli is given by Eq. (15) with $n = 1$, $\epsilon_0 = 1.0$, and $\epsilon_1 = 0.481$ ($\kappa = 0.42$). It is evident from Figure 6 that deviation from linearity occurs for high Re numbers.

For power-law fluids, the entrance correction versus Re is shown in Figure 7. Due to the generalized Reynolds number employed [Eq. (15)], the curves for different power-law indices n come much closer together than by using a standard Re without taking into account the effect of shear thinning and geometry (e.g., the one used by Kim-E et al.[8]). However, even using a generalized Re, it is obvious that the lines have different slopes and intercepts for different values of n, as shown in Figure 8. For Re $\leq$ 200, the correspond-

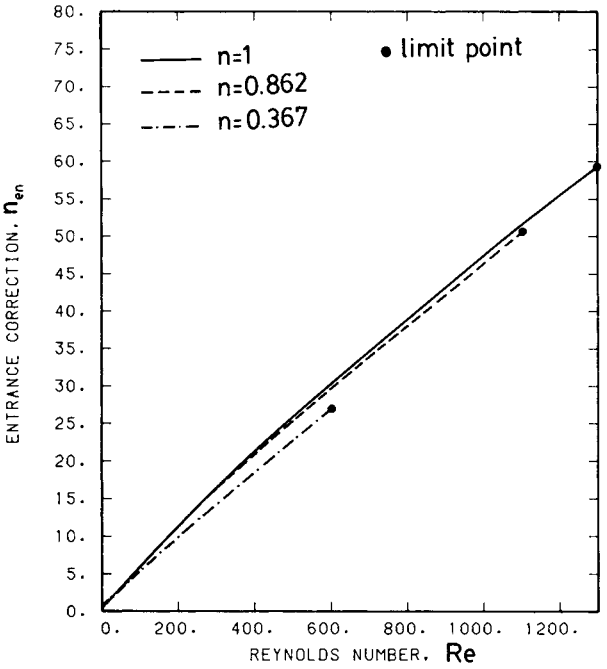

Fig. 7. Entrance correction vs. Re number (power-law fluids in a 2 : 1 annular abrupt contraction). —, $n = 1$; - - -, $n = 0.862$; - · -, $n = 0.367$.

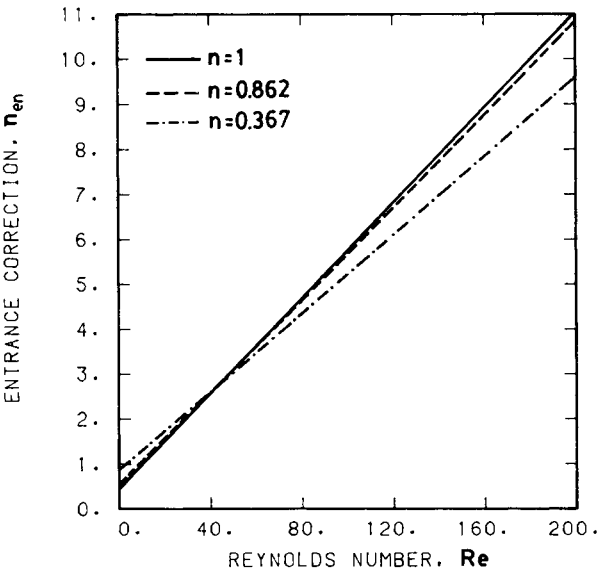

Fig. 8. Entrance correction of power-law fluids for low Re numbers (blown-up section of Fig. 7).

ing equations are:

$$(n = 0.862) \qquad n_{en} = 0.051\ \mathrm{Re} + 0.570 \tag{26}$$

$$(n = 0.367) \qquad n_{en} = 0.043\ \mathrm{Re} + 0.895 \tag{27}$$

For higher values of Re, the above equations give overestimates of the actual values. These overestimates increase with increasing Re numbers.

Viscoelastic Fluids

The effect of viscoelasticity was examined first in the absence of inertia (Re = 0) for the test fluid FS8, obeying the power-law relationships given by Eqs. (22a–d). The creeping flow patterns for increasing Ws numbers are shown in Figure 9. The reservoir corner vortex increases dramatically with Ws, both

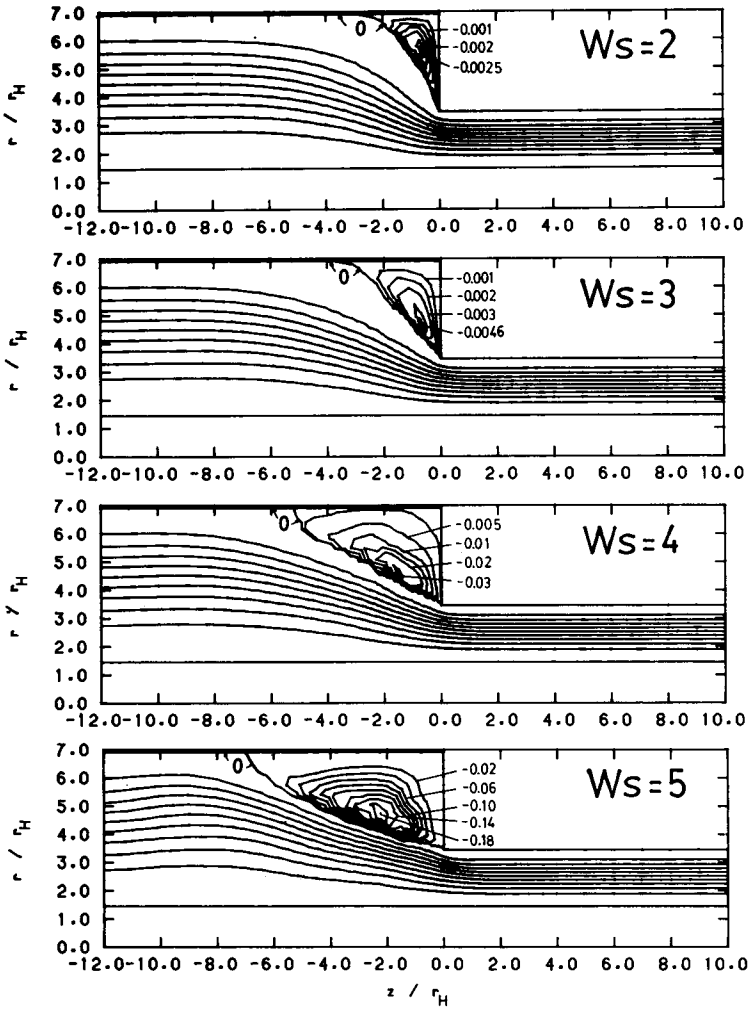

Fig. 9. Creeping flow patterns of test fluid FS8 for different Ws numbers (Re = 0).

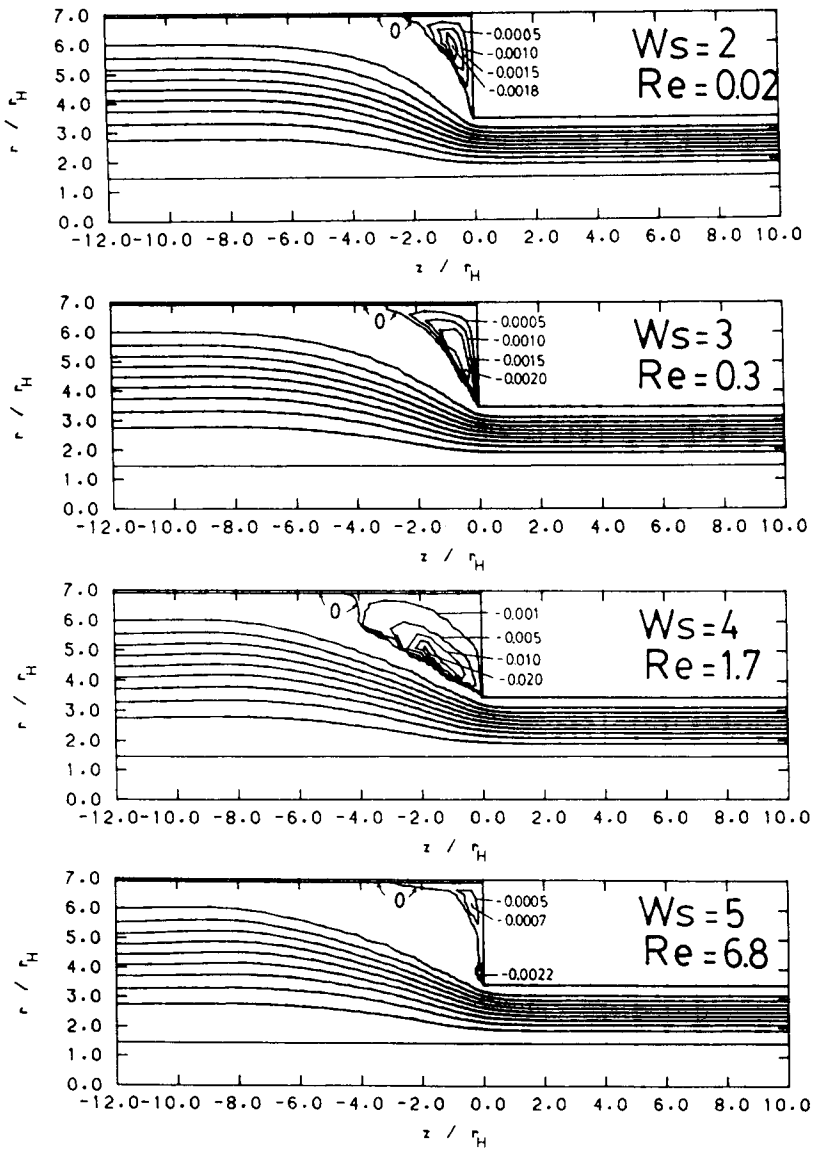

Fig. 10. Flow patterns of test fluid FS8 for different Re and Ws numbers.

in size and intensity. Similar behavior has also been found in creeping flows of viscoelastic fluids through capillaries and slits.[2,3,10] The intensity increases from the essentially Newtonian value of -0.0011 for Ws = 0 to -0.18 for Ws = 5. The corresponding values of the dimensionless vortex length X_v are 0.135 for Ws = 0 and 0.64 for Ws = 5. It is interesting to note that the macroscopic Deborah number Ws/X_v for these runs obeys the relation:[14,26]

$$\lim_{\mathrm{Re}\to 0} \mathrm{Ws}/X_v = 8.0 \tag{28}$$

within $\pm 3\%$. For Ws = 5, a limit point was encountered, above which the solution diverged.

Finally, the combined effect of inertia and viscoelasticity was studied for the test fluid FS8. The flow patterns are shown in Figure 10 for increasing Re and Ws numbers. Unfortunately, due to convergence problems for Ws > 5, we were not able to obtain the flow patterns for exactly the same conditions as these shown by Tan and Tiu.[14] However, the general trends are clearly demonstrated in the present simulations, that is, at first there is a vortex growth regime as Re and Ws increase, followed by a divergent flow regime (bending of the streamlines) and a substantial reduction in the size and intensity of the reservoir vortex which now grows from the re-entrant corner (Re = 6.8, Ws = 5). The influence then of inertia is to reduce the vortex that otherwise would have been much greater (compare with Fig. 9 for Ws = 5).

The discrepancies between the present flow patterns and the ones found experimentally by Tan and Tiu[14] for fluid FS8 can be attributed mainly to the inadequacy of the viscometric approximation approach used to treat the viscoelastic terms and to a lesser extent to the lack of experimental data for the full range of shear rates (both at very low and at very high $\dot{\gamma}$ values). As explained earlier,[3] the viscometric approximation fails to account for elongational effects, that apparently play quite an important role in entry flows. Experimental data on the elongational viscosity are also lacking for fluid FS8. However, we feel that the current approach at least qualitatively captures the dramatic changes caused by the combined effect of inertia and viscoelasticity in the entry flow through the annular abrupt contraction.

CONCLUSIONS

The behavior of Newtonian, power-law, and viscoelastic fluids in entry flows through a 2:1 annular abrupt contraction has been simulated numerically using the finite-element method. The influence of inertia and viscoelasticity as measured by a generalized Reynolds (Re) and Weissenberg (Ws) numbers, respectively, has been studied by decoupling these effects.

Inertia in the absence of viscoelasticity (Ws = 0) was found to decrease the reservoir corner vortex for Re $\leq$ 200, after which an increase takes place to produce a small but elongated vortex. At values of Re ~ 200, a vena contracta appears in the downstream channel, which grows with Re. The pressures were used to evaluate the excess pressure losses or entrance correction n_{en} due to the contraction. The results showed a linear dependence on Re for Re $\leq$ 200, that depends on the power-law index n. However, the use of a generalized Re number that takes into account the effect of shear thinning and geometry, brings the results much closer together. A limit point for convergence was found at Re_c = 1300 for Newtonian fluids. The limit point decreases with the power-law index n (R_c = 600 for n = 0.367). The high values of Re numbers reached in the present work are apparently due to a continuation solution scheme, a dense finite element grid, and the 2:1 contraction ratio which is not very severe.

The effect of viscoelasticity (Ws $\neq$ 0) was studied by using a simplified model based on the viscometric approximation approach.[3] In the absence of inertia (Re = 0), it was found that the reservoir corner vortex increases dramatically with Ws, both in intensity and size, as measured by a dimension-

less vortex length X_v. However, the ratio Ws/X_v was found to equal 8, in agreement with experimental evidence.[14,26] A limit for convergence was also found at $Ws_c = 5$.

The combined effect of inertia and viscoelasticity ($Re \neq 0$, $Ws \neq 0$) was found to be such that at moderate Re and Ws numbers there is a vortex growth regime, accompanied by a divergent flow regime and substantial reduction in the vortex size as Re and Ws increase. These findings are in qualitative agreement with experimental evidence available in the literature.[14]

Financial assistance from the Natural Sciences and Engineering Research Council of Canada (NSERC) is gratefully acknowledged.

References

1. S. A. White, A. D. Gotsis, and D. G. Baird, *J. Non-Newt. Fluid Mech.*, **24**, 121 (1987).
2. E. Mitsoulis, J. Vlachopoulos, and F. A. Mirza, *Polym. Eng. Sci.*, **25**, 677 (1985).
3. E. Mitsoulis, *Polym. Eng. Sci.*, **26**, 1552 (1986).
4. D. V. Boger, *Adv. Transp. Proc.*, **2**, 43 (1982).
5. D. V. Boger, R. Gupta, and R. I. Tanner, *J. Non-Newt. Fluid Mech.*, **4**, 239 (1978).
6. E. Mitsoulis, J. Vlachopoulos, and F. A. Mirza, *Polym. Eng. Sci.*, **24**, 707 (1984).
7. C. A. Hieber, *Rheol. Acta*, **26**, 92 (1987).
8. M. E. Kim-E, R. A. Brown, and R. C. Armstrong, *J. Non-Newt. Fluid Mech.*, **13**, 341 (1983).
9. E. Mitsoulis and J. Vlachopoulos, *AIChE J.*, **31**, 1736 (1985).
10. E. Mitsoulis, J. Vlachopoulos, and F. A. Mirza, *J. Appl. Polym. Sci.*, **30**, 1379 (1985).
11. M. J. Crochet and G. Pilate, *J. Non-Newt. Fluid Mech.*, **1**, 247 (1976).
12. M. G. N. Perera and K. Strauss, *J. Non-Newt. Fluid Mech.*, **5**, 269 (1979).
13. K. L. Tan and C. Tiu, *J. Non-Newt. Fluid Mech.*, **3**, 25 (1977/1978).
14. K. L. Tan and C. Tiu, *J. Non-Newt. Fluid Mech.*, **6**, 21 (1979).
15. R. B. Bird, W. E. Stewart, and E. N. Lightfoot, *Transport Phenomena*, Wiley, New York, 1960.
16. R. B. Bird, R. C. Armstrong, and O. Hassager, *Dynamics of Polymeric Liquids*, Vol. I, Wiley, New York, 1977.
17. M. Keentok, A. G. Georgesen, A. A. Sherwood, and R. I. Tanner, *J. Non-Newt. Fluid Mech.*, **6**, 303 (1980).
18. K. P. Jackson, K. Walters, and R. W. Williams, *J. Non-Newt. Fluid Mech.*, **14**, 173 (1984).
19. W. Kozicki and C. Tiu, *Can. J. Chem. Eng.*, **49**, 562 (1971).
20. A. G. Fredrickson and R. B. Bird, *Ind. Eng. Chem.*, **50**, 347 (1958).
21. E. Mitsoulis, J. Vlachopoulos, and F. A. Mirza, "MACVIP-A Finite Element Program for Creeping Viscoelastic Flows," Internal Report, Faculty of Engineering, McMaster University, Hamilton, Ontario, Canada (1983).
22. E. Mitsoulis and J. Vlachopoulos, *Adv. Polym. Techn.*, **4**, 107 (1984).
23. K. L. Tan, Ph.D. thesis, Dept. Chem. Eng., Monash University, Clayton, Victoria, Australia, 1977.
24. D. V. Boger, D. U. Hur, and R. J. Binnington, *J. Non-Newt. Fluid Mech.*, **20**, 31 (1986).
25. E. B. Christiansen, S. J. Kelsey, and T. R. Carter, *AIChE J.*, **18**, 372 (1972).
26. P. J. Cable and D. V. Boger, *AIChE J.*, **24**, 869, 992 (1978).

Received July 22, 1987
Accepted September 29, 1987